FULL PAPER

Synthesis, Structure, and Spectroscopic Properties of the New Lanthanum(III) Fluoride Oxomolybdate(VI) La$_3$FMo$_4$O$_{16}$

Ingo Hartenbach,*[a] Sabine Strobel,[a,b] Thomas Schleid,[a] Biprajit Sarkar,[a] Wolfgang Kaim,[a] Peter Nockemann,[c] Koen Binnemans,[c] and Peter K. Dorhout[b]

La$_3$FMo$_4$O$_{16}$ crystallizes in the triclinic crystal system with space group $P\bar{1}$ [a = 724.86(2) pm, b = 742.26(2) pm, c = 1469.59(3) pm, α = 101.683(2)°, β = 102.118(2)°, γ = 100.279(2)°] with two formula units per unit cell. The three crystallographically independent La^{3+} cations show a coordination number of nine each, with one F$^-$ and eight O^{2-} anions forming distorted monocapped square antiprisms. The fluoride anion is coordinated by all three lanthanum cations to form a nearly planar triangle. Besides three crystallographically independent tetrahedral [MoO$_4$]$^{2-}$ units, a fourth one with a higher coordination number (CN = 4 +1) can be found in the crystal structure, forming a dimeric entity with a for-

mula of [Mo$_2$O$_8$]$^{4-}$ consisting of two edge-connected square pyramids. Several spectroscopic measurements were performed on the title compound, such as infrared, Raman, and diffuse reflectance spectroscopy. Furthermore, La$_3$FMo$_4$O$_{16}$ was investigated for its capacity to work as host material for doping with luminescent active cations, such as Ce^{3+} or Pr^{3+}. Therefore, luminescence spectroscopic as well as EPR measurements were performed with doped samples of the title compound. Both the pure and the doped compounds can be synthesized by fusing La$_2$O$_3$, LaF$_3$ and MoO$_3$ (ratio 4:1:12; ca. 1 % CeF$_3$ and PrF$_3$ as dopant, respectively) in evacuated silica ampoules at 850 °C for 7 d.

Introduction

The quest for energy efficient materials has become a serious issue for saving this planet from global warming. One major point hereby is low-energy illumination for almost every area in today's life (e.g. ambient lighting, automobile and traffic lights, scintillation materials for detectors, etc.). Thus, the interest in new luminescent materials is constantly increasing, considering the rapid development of efficient energy delivering technologies (e.g. new LEDs, etc.). Luminescent materials usually consist of an innocent (i.e. *non*-luminescent) host and a luminescence-active dopant. Trivalent lanthanoid cations are a good choice as dopants, although most of them (e.g. Eu^{3+}, Tb^{3+}, etc.) obtain their activity from spin-forbidden f–f transitions, which are less efficient than the spin-permitted f–d transitions of Eu^{2+} for example. With an array of proper working dopants at hand, finding a good host material is one of the major challenges in the design of luminescent materials. Oxomolybdate derivatives of lanthanum and yttrium[1] are usu-

ally very promising candidates for this task, because they provide *non*-luminescent cations with a size comparable to, and thus substitutable by other lanthanoid trications. A lot of cationic oxomolybdate derivatives and their properties have already been published (e.g. KLa[MoO$_4$]$_2$:Tb^{3+},[2] Na-La[MoO$_4$]$_2$:Tm^{3+},[3] etc.). They usually crystallize in a *scheelite*-type structure[4] or one of its variations. A different approach is chosen in this work, since the title compound represents an anionic derivative of a rare-earth metal(III) oxomolybdate(VI), not a cationic one. The insertion of a halide anion is a facile way to synthesize derivatives with new structures and interesting properties. The simplest formula to achieve is *RE*X[MoO$_4$] (*RE* = Y, La–Nd, Sm–Lu; X = F,[1,5] Cl,[6–8] Br[9]). The title compound La$_3$FMo$_4$O$_{16}$ exhibits a new, fluorine-poorer composition, formally according to LaF[MoO$_4$]×La$_2$[MoO$_4$]$_3$,[10] which is a promising host material for luminescence properties. Therefore, it was doped with Ce^{3+} (to synthesize a potential scintillator material) and Pr^{3+} cations (which provide luminescence both in the red and green range, depending on the oxidation state of praseodymium), which both have a similar size to La^{3+} cations and should thus be able to substitute them very well. The major advantage of the title compound as host material is the fact, that the doped cation has not to be excited directly (usually in a very small energetic range), but the excitation can also take place in the region of the broad O–Mo charge-transfer band. Hence, oxomolybdate units provide a so-called "inorganic antenna effect".

[a] Institut für Anorganische Chemie, Universität Stuttgart,
Pfaffenwaldring 55, 70569 Stuttgart, Germany
Fax: +49-711-6855-4254
E-mail: hartenbach@iac.uni-stuttgart.de
[b] Department of Chemistry, Colorado State University,
Fort Collins, 80523, CO, USA
[c] Department of Chemistry, Katholieke Universiteit Leuven,
3000 Leuven, Belgium

Results and Discussion

Crystal Structure

La$_3$FMo$_4$O$_{16}$ crystallizes in the triclinic system with space group $P\bar{1}$ [a = 724.86(2) pm, b = 742.26(2) pm, c = 1469.59(3) pm, α = 101.683(2)°, β = 102.118(2)°, γ = 100.279(2)°] with two formula units per unit cell. In the structure three crystallographically different La^{3+} cations can be distinguished, which are surrounded by one F$^-$ and eight O^{2-} anions each in the shape of distorted monocapped square antiprisms (Figure 1, *top left, top right*, and *bottom left*). The distances between La^{3+} and F$^-$ [d(La^{3+}–F$^-$) = 243–250 pm] within these polyhedra are situated in the same range as in the respective binary compound LaF$_3$ [d(La^{3+}–F$^-$) = 242–264 pm].[11] This is not true for the La^{3+}–O^{2-} distances [d(La^{3+}–O^{2-}) = 242–299 pm], since they exceed those of La$_2$O$_3$ [d(La^{3+}–O^{2-}) = 237–245 pm][12] and La$_2$[MoO$_4$]$_3$ [d(La^{3+}–O^{2-}) = 244–259 pm][10] by about 16%. Nonetheless, the oxide anions with the longer distances provide a small but not negligible contribution to the effective coordination numbers ECoN[13] of the lanthanum cations [e.g. the longest distance (La1)$^{3+}$–(O5)$^{2-}$ displays a share of 0.18 to the effective coordination number of 7.81 for La1]. The fluoride anions are surrounded by each of the three crystallographically independent La^{3+} cations, forming a triangle with the formula [FLa$_3$]$^{8+}$ in which the F$^-$ anions reside 24 pm above the triangular plane (Figure 1, *bottom right*).
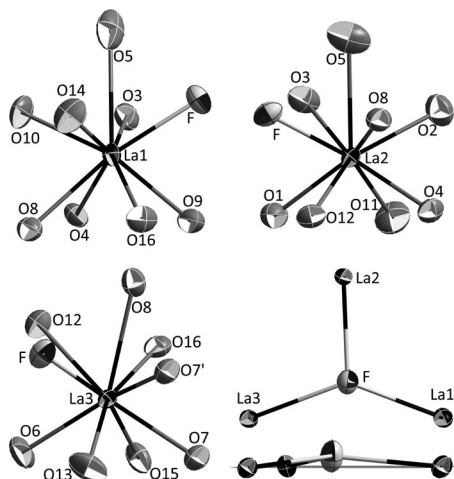

Figure 1. Anionic coordination environment around the (La1)$^{3+}$, *top left*, (La2)$^{3+}$, *top right*, and (La3)$^{3+}$ cations, *bottom left*, as well as the cationic surrounding of the F$^-$ anions, *bottom right*, emphasizing the small displacement of the fluoride anions from the triangular plane in the crystal structure of La$_3$FMo$_4$O$_{16}$.

Four crystallographically distinguishable oxomolybdate(VI) units are found in the crystal structure of the title compound. While the polyhedra around Mo1, Mo2, and Mo3 correspond to *ortho*-oxomolybdate entities [MoO$_4$]$^{2-}$ (Figure 2, *top left, top right* and *middle*), the fourth molybdenum cation shows a coordination number of four *plus one* in the shape of a distorted square pyramid. Two of these [(Mo4)O$_{4+1}$]$^{4-}$ units are fused together via one common

edge to form a dimer [(Mo4)$_2$O$_8$]$^{4-}$ with an inversion center in the middle of the connecting edge (Figure 2, *bottom*). The Mo^{6+}–O^{2-} bond lengths range between 173 and 180 pm *plus* a longer one between (Mo4)$^{6+}$ and (O15′)$^{2-}$ of 235 pm. The shorter distances are in good agreement with those of other oxomolybdates consisting of simpler tetrahedral [MoO$_4$]$^{2-}$ entities (e.g. La$_2$[MoO$_4$]$_3$: d(Mo^{6+}–O^{2-}) = 173–182 pm).[10] Whenever the molybdate units show an enhancement of their coordination number from four to five with one longer distance, the latter ranges in an interval between 230 and 245 pm (e.g. Sm$_2$Mo$_3$O$_{12}$ exhibits a long, fifth Mo^{6+}–O^{2-} distance of almost 242 pm and can therefore not be addressed as Sm$_2$[MoO$_4$]$_3$).[14] Thus, the observed distance of 235 pm in the title compound is in good agreement with related compounds. Although the contribution of this fifth, longer bonding association to the effective coordination number (ECoN)[13] of (Mo4)$^{6+}$ [δ(ECoN)$_{Mo4–O15'}$ = 0.014 to ECoN$_{Mo4}$ = 3.9604], as well as to the valence state of Mo4 (bond valence contribution of O15′ = 0.332 to the valence sum of Mo4, amounts to 6.037)[15–17] is rather small, this distance cannot be neglected, since the fifth ligand explains the deviation of the remaining four short-bonded oxygen atoms from the ideal tetrahedral arrangement (Table 1).
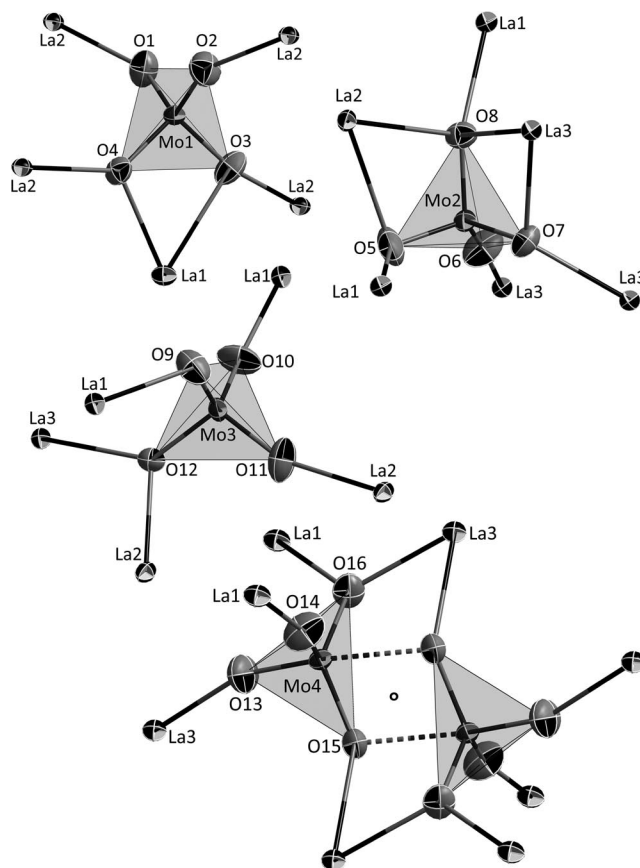

Figure 2. Cationic coordination environment around the [(Mo1)-O$_4$]$^{2-}$, *top left*, [(Mo2)O$_4$]$^{2-}$, *top right*, and [(Mo3)O$_4$]$^{2-}$ anions, *middle*, as well as around the dimer [(Mo4)$_2$O$_8$]$^{4-}$ of two edge-shared quadrangular pyramids, *bottom*, emphasizing their arrangement at the inversion center represented by the *Wyckoff* position 1g.

Table 1. Interatomic distances (d/pm, esd = ±0.1) and selected bond angles ($\angle$/deg, esd = ±0.1) for $La_3FMo_4O_{16}$.

	d/pm		d/pm		d/pm
La1 – F	243.0	La2 – F	249.3	La3–F	250.2
La1–O10	242.1	La2–O3	244.3	La3–O6	242.4
La1–O14	243.5	La2–O11	244.4	La3–O16	251.7
La1–O16	251.7	La2–O2	247.7	La3–O7	252.1
La1–O4	253.6	La2–O4	247.7	La3–O13	252.5
La1–O9	256.5	La2–O1	248.2	La3–O12	253.3
La1–O8	269.5	La2–O12	255.0	La3–O15	255.3
La1–O3	282.2	La2–O8	268.9	La3–O7	271.0
La1–O5	299.5	La2–O5	288.2	La3–O8	281.2

	d/pm		d/pm
Mo1–O1	173.5	Mo2–O5	174.0
Mo1–O2	173.8	Mo2–O6	174.8
Mo1–O3	178.1	Mo2–O7	177.9
Mo1–O4	180.1	Mo2–O8	179.0
Mo3–O9	174.1	Mo4–O13	173.5
Mo3–O10	175.0	Mo4–O14	173.5
Mo3–O11	175.0	Mo4–O15	181.9
Mo3–O12	179.8	Mo4–O16	182.4
		Mo4–O15′	234.1

	$\angle$/deg		$\angle$/deg
O1–Mo1–O2	108.7	O5–Mo2–O6	114.2
O1–Mo1–O3	112.9	O5–Mo2–O7	109.2
O1–Mo1–O4	111.1	O5–Mo2–O8	103.3
O2–Mo1–O3	111.1	O6–Mo2–O7	112.2
O2–Mo1–O4	114.8	O6–Mo2–O8	115.3
O3–Mo1–O4	98.3	O7–Mo2–O8	101.6
O9–Mo3–O10	112.7	O13–Mo4–O14	105.2
O9–Mo3–O11	110.7	O13–Mo4–O15	100.2
O9–Mo3–O12	106.3	O13–Mo4–O15′	168.5
O10–Mo3–O11	109.1	O13–Mo4–O16	100.0
O10–Mo3–O12	110.4	O14–Mo4–O15	112.9
O11–Mo3–O12	107.6	O14–Mo4–O15′	86.3
		O14–Mo4–O16	110.2
		O15–Mo4–O15′	73.9
		O15–Mo4–O16	124.9
		O15′–Mo4–O16	76.3

Figure 3. View at the crystal structure of $La_3FMo_4O_{16}$ along [010], *top*, and [100], *bottom*, with special emphasis on the triangular $[FLa_3]^{8+}$ units (*dark grey triangles*) and their two-dimensional, hexagonally close-packed arrangement parallel to the (100) plane.

The crystal structure is best described using the complex units $[MoO_4]^{2-}$, $[Mo_2O_8]^{4-}$, and $[FLa_3]^{8+}$ as building blocks. The fluoride-centered triangles are spread two-dimensionally throughout the (100) plane, enclosing an angle of 36° with it (Figure 3, *top*). The arrangement of the $[FLa_3]^{8+}$ units resembles a hexagonally close-packed layer, when viewed along the *a*-axis, with the molybdate units spreading in all three dimensions as anionic neighbors of the triangular complex cations $[FLa_3]^{8+}$ (Figure 3, *bottom*). The aforementioned $[(Mo4)_2O_8]^{4-}$ double-pyramids are arranged around the inversion center at the 1*g* *Wyckoff* position (0, 1/2, 1/2). Hence, the formula can be written as $[La_3F]_2$-$[MoO_4]_6[Mo_2O_8]$, emphasizing that the structure is built completely of these complex units. Structures containing oxomolybdate units can very often be compared to those with analogous complex anions of the sixth and sixteenth group (e.g. oxotungstates, oxosulfates, etc.), due to a similar steric behavior and electronic charge. However, in case of $La_3FMo_4O_{16}$, there is no compound with an analogous composition $RE_3FM_4O_{16}$ (RE = rare-earth metal trication, M = group six or sixteen hexacation) known so far. Only

Table 2. Motifs of mutual adjunction[27] for $La_3FMo_4O_{16}$.

	La1	La2	La3	Mo1	Mo2	Mo3	Mo4	CN
F	1/1	1/1	1/1	0/0	0/0	0/0	0/0	3
O1	0/0	1/1	0/0	1/1	0/0	0/0	0/0	2
O2	0/0	1/1	0/0	1/1	0/0	0/0	0/0	2
O3	1/1	1/1	0/0	1/1	0/0	0/0	0/0	3
O4	1/1	1/1	0/0	1/1	0/0	0/0	0/0	3
O5	1/1	1/1	0/0	0/0	1/1	0/0	0/0	3
O6	0/0	0/0	1/1	0/0	1/1	0/0	0/0	3
O7	0/0	0/0	2/2	0/0	1/1	0/0	0/0	3
O8	1/1	1/1	1/1	0/0	1/1	0/0	0/0	4
O9	1/1	0/0	0/0	0/0	0/0	1/1	0/0	2
O10	1/1	0/0	0/0	0/0	0/0	1/1	0/0	2
O11	0/0	1/1	0/0	0/0	0/0	1/1	0/0	2
O12	0/0	1/1	1/1	0/0	0/0	1/1	0/0	3
O13	0/0	0/0	1/1	0/0	0/0	0/0	1/1	2
O14	1/1	0/0	0/0	0/0	0/0	0/0	1/1	2
O15	0/0	0/0	1/1	0/0	0/0	0/0	1+1/1+1	2+1
O16	1/1	0/0	1/1	0/0	0/0	0/0	1/1	3
CN	9	9	9	4	4	4	4+1	

the oxoselenates(IV) with the formula RE_3F[SeO$_3$]$_4$ ($RE =$ Pr, Nd, Sm–Ho)[18–21] can be compared to the title compound, solely by the fact that these consist of [FRE_3]$^{8+}$ triangles (similar to the [FLa$_3$]$^{8+}$ units in La$_3$FMo$_4$O$_{16}$) and ψ^1-tetrahedral [SeO$_3$]$^{2-}$ units with about the same steric demand as the genuine tetrahedral [MoO$_4$]$^{2-}$ entities. However, the structural arrangement of the aforementioned building blocks in the RE_3F[SeO$_3$]$_4$-type phases is completely different (Table 2).

Infrared and Raman Spectroscopy

Both the infrared and the Raman spectra of La$_3$F-Mo$_4$O$_{16}$ were taken from finely powdered samples of the bulk substance. The infrared spectrum of the title compound (Figure 4, *top*) shows a weak but broad band at 1100 cm^{-1}, corresponding to the antisymmetric stretching vibration of β-cristobalite type SiO$_2$,[22] thus, a small impurity of silicon dioxide is assumed to be present in all our samples (as one might expect from the synthesis within silica ampoules), which is also confirmed by X-ray powder diffraction data. It was also observed in the vibrational spectra of the fluoride oxomolybdates of the smaller lanthanides REF[MoO$_4$] (RE = Sm – Tm),[5] where the same bands, only of stronger intensities, were observed as well. The stretching vibrations of tetrahedral [MoO$_4$]$^{2-}$ anions are usually found in the energy range between 760 and

980 cm^{-1}, which can clearly be seen in both spectra. Furthermore, the Raman spectrum allows one to distinguish between the more intense symmetric stretching vibration,[23,24] which can be found at higher energies (900–980 cm^{-1}), and the less intense modes at smaller wavenumbers (760–880 cm^{-1}) resulting from the antisymmetric stretching of the oxomolybdate(VI) tetrahedra. The deformation vibrations of molybdate units are generally situated between 200 and 400 cm^{-1}; however, in this range La–O and La–F stretching modes are also found, thus, an explicit assignment of the bands below 400 cm^{-1} is hardly possible. The same is probably true for the stretching vibration of the long Mo4–O15′ "bond". The latter can not necessarily be considered covalent but rather ionic. Therefore its force constant should be situated in the area of other interactions driven by Coulomb force, like those between La^{3+} cations and F$^-$/O^{2-} anions.

Luminescence Spectroscopy

The luminescence spectrum of La$_3$FMo$_4$O$_{16}$:Pr^{3+} was determined from the solid state and is shown in Figure 5 (*top*). The compound exhibits orange-red luminescence under UV irradiation. The luminescence spectrum of La$_3$FMo$_4$-O$_{16}$:Pr^{3+} presents the typical transitions for praseodymium with the three dominant energy bands ^{3}P$_0$ → ^{3}H$_6$ at 16570 cm^{-1} (602 nm), ^{3}P$_0$ → ^{3}H$_4$ at 20520 cm^{-1} (487 nm), and ^{3}P$_0$ → ^{3}F$_2$ at 15434 cm^{-1} (647 nm). Besides those, the transitions of ^{3}P$_0$ → ^{3}H$_5$ at 18853 cm^{-1} (531 nm), ^{3}P$_0$ → ^{3}F$_3$ at 14400 cm^{-1} (694 nm), and ^{3}P$_0$ → ^{3}F$_4$ at 13677 cm^{-1} (731 nm) can be observed. The luminescence decay of the ^{3}P$_0$ excited state [monitored via the ^{3}P$_0$ → ^{3}H$_6$ transition at 16570 cm^{-1} (602 nm), upon excitation into the ^{3}P$_2$ level at 22464 cm^{-1} (447 nm)] was found to be single exponential and the radiative lifetime can thus be determined to 36 μs. The excitation spectrum [performed by monitoring the ^{3}P$_0$ → ^{3}H$_6$ emission at 16570 cm^{-1} (602 nm), see Figure 5, *bottom*] exhibits a broad band besides the typical finely-resolved f–f transition lines of praseodymium (^{3}P$_2$ ← ^{3}H$_4$, ^{3}P$_1$, ^{1}I$_6$ ← ^{3}H$_4$, ^{3}P$_0$ ← ^{3}H$_4$).

The broad band between 250 and 340 nm can be attributed mainly to the O → Mo ligand-to-metal charge transfer (LMCT) transition. Excitation at 290 nm into this charge-transfer band results in an emission spectrum, which does not show significant differences to the excitation at 447 nm. Therefore, there is the distinct possibility to use this wide range for excitation, the so-called "inorganic antenna effect". Although this effect is observed in this system, the efficiency is low, which can be deduced from the fact, that the f–f transitions of Pr^{3+} are clearly visible in the excitation spectrum. In case of a high efficiency only an intense charge-transfer band would be visible and the f–f transitions were weak and hard to detect. The explanation for the low efficiency antenna effect lies within an energetic mismatch between the LMCT band and the ^{4}F$_2$ levels of Pr^{3+}. With the exception of the ^{1}S$_0$ state at very high energy (> 50000 cm^{-1}) there are no energy levels above the ^{3}P$_2$

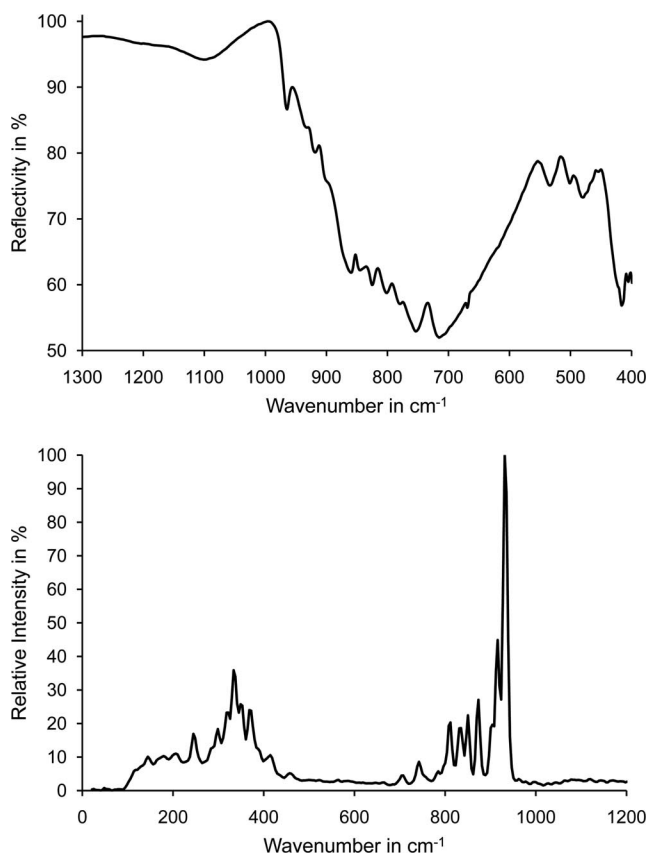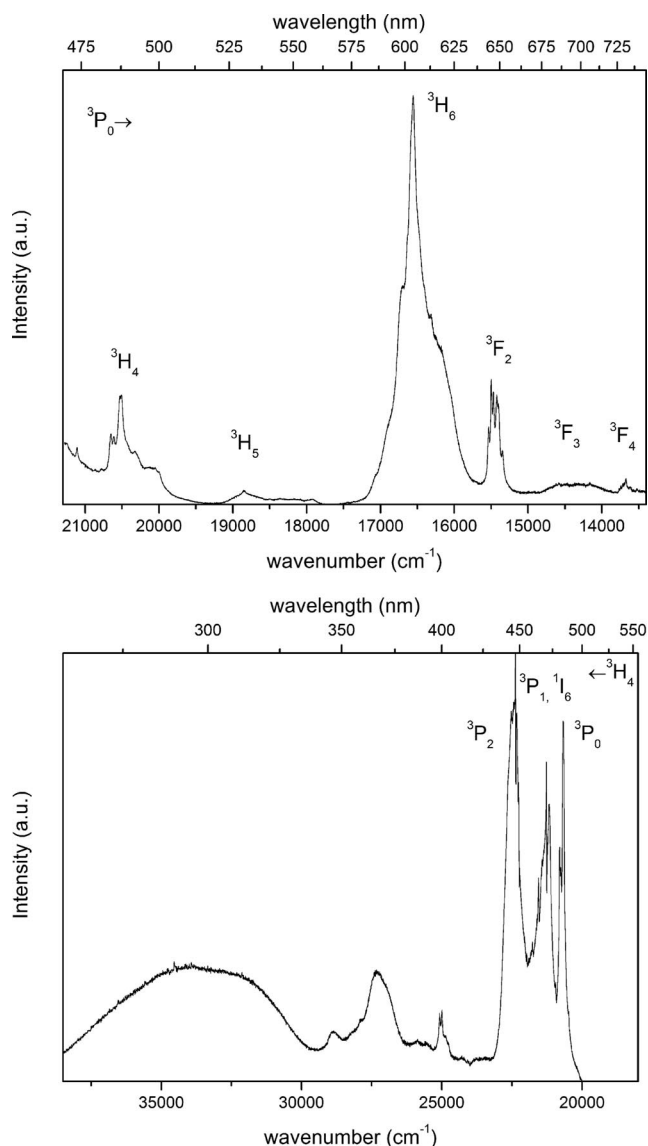Figure 4. Infrared, *top*, and Raman spectrum, *bottom*, of solid La$_3$FMo$_4$O$_{16}$.

Figure 5. Emission (λ_{exc} = 447 nm), *top*, and excitation spectrum (λ_{em} = 602 nm), *bottom*, with special emphasis on the broad band at about 300 nm in the latter, representing the O → Mo ligand-to-metal charge transfer (LMCT) transitions of the oxomolybdate(VI) units.

state, which is situated at much lower energy than the charge-transfer state. La$_3$FMo$_4$O$_{16}$:Ce^{3+} was also investigated, with the idea of using this compound as a potential new material in scintillation detectors; unfortunately, no such properties were detected. Two possible explanations can be given for the optical silence of the Ce^{3+}-doped substance. First, Ce^{3+} cations were not really inserted into the structure, a hypothesis that was disproved by EPR spectroscopy (see next section). Therefore, the second explanation seems to be the correct one, which proclaims that the LMCT bands of the oxomolybdate(IV) units are situated below the emitting level of Ce^{3+}.

Electron Paramagnetic Resonance Spectroscopy

The EPR spectra of the Ce^{3+}- and Pr^{3+}-doped title compound were recorded in the solid state at 4 K. The spectra

of both compounds show a large splitting of the *g*-components (Figure 6). La$_3$FMo$_4$O$_{16}$:Ce^{3+} exhibits the following anisotropic *g*-values: g_1 = 5.56, g_2 = 1.88, g_3 = 1.16 (Δg = 4.40, g_{iso} = 2.87), while those of La$_3$FMo$_4$O$_{16}$:Pr^{3+} yield g_1 = 5.44, g_2 = 1.21 and g_3 = 0.85 (Δg = 4.59, g_{iso} = 2.50). The unpaired electrons of both substances occupy f-orbitals which are apparently not influenced by any ligand field, and hence remain degenerated. This behaviour is very common, since the f-orbitals are situated close to the atomic core and therefore are not affected by the ligand-field, which is contrary to the observations for d-orbitals. Such a degenerate situation obviously leads to the large *g*-anisotropy and average *g*-values for both La$_3$FMo$_4$O$_{16}$:Ce^{3+} and La$_3$FMo$_4$O$_{16}$:Pr^{3+}. The expected hyperfine coupling to the nuclear spin of Pr^{3+} could not be resolved. This is probably due to line broadening in the powder form arising out of dipolar interactions.
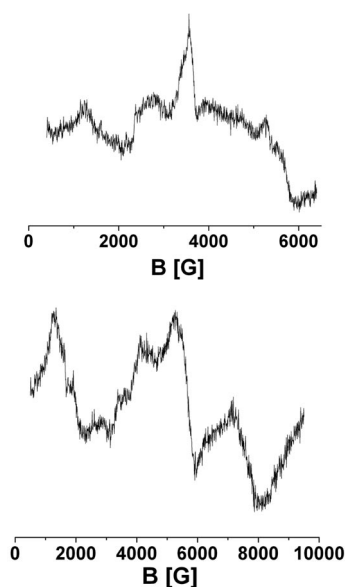

Figure 6. EPR spectrum of La$_3$FMo$_4$O$_{16}$:Ce^{3+}, *top*, and La$_3$FMo$_4$O$_{16}$:Pr^{3+} *bottom*.

Conclusions

The new lanthanum(III) fluoride oxomolybdate(VI) La$_3$FMo$_4$O$_{16}$ was synthesized as bulk compound, as well as being doped with Ce^{3+} and Pr^{3+} cations, by means of solid-state reactions from admixtures of La$_2$O$_3$, LaF$_3$, and MoO$_3$. Its crystal structure was determined by single-crystal X-ray structure analysis and X-ray powder diffraction was performed to investigate the phase purity. Three main building blocks, [MoO$_4$]$^{2-}$ and [Mo$_2$O$_8$]$^{4-}$ anions as well as [FLa$_3$]$^{8+}$ cations, were identified as key building units in the crystal structure. Several spectroscopy methods were used to probe the properties of finely powdered samples comprising both the bulk and the two doped substances. As one result, La$_3$FMo$_4$O$_{16}$ appears to be a suitable host material for luminescence applications, in providing an "inorganic antenna effect", owing to the charge transfer transitions within the oxomolybdate(VI) units.

Experimental Section

Synthesis: La$_3$FMo$_4$O$_{16}$ was obtained by the reaction of a mixture of lanthanum trifluoride (LaF$_3$: 99.9%; ChemPur, Karlsruhe, Germany), lanthanum sesquioxide (La$_2$O$_3$: 99.9%; ChemPur, Karlsruhe, Germany) and molybdenum trioxide (MoO$_3$: p. a. quality; Merck, Darmstadt, Germany) with the three components in the molar ratio of 1:4:12 in evacuated silica ampoules for seven days at 850 °C according to the equation below.

$$\text{LaF}_3 + 4\ \text{La}_2\text{O}_3 + 12\ \text{MoO}_3 \rightarrow 3\ \text{La}_3\text{FMo}_4\text{O}_{16}$$

From this reaction, transparent, colorless, bulky single crystals emerged, which remained stable in air and water. To synthesize doped compounds, about 1% of CeF$_3$ or PrF$_3$, respectively, was added to the initial reaction mixture, replacing adequate amounts of LaF$_3$. Although, lanthanum trifluoride is notorious for attacking the wall of silica containers, the contamination of the bulk substance with SiO$_2$ or binary silicates is extremely small, according to infrared spectroscopy and cannot be detected with X-ray powder diffractometry.

X-ray Crystallography: The X-ray powder diffraction pattern was measured with a Stoe STADI P diffractometer with a position-sensitive detector using germanium-monochromatized Cu-K_α radiation (λ = 154.06 pm). The powder diffractogram of La$_3$FMo$_4$O$_{16}$, together with the corresponding theoretical powder pattern calculated from the single-crystal data, was deposited as supplementary material. Intensity data sets for single crystals of La$_3$FMo$_4$O$_{16}$ were collected with a Nonius Kappa-CCD diffractometer using graphite-monochromatized Mo-K_α radiation (wavelength: λ = 71.07 pm). Numerical absorption correction was performed with the help of the program HABITUS.[25] The structure solution and refinement was carried out by using the program package SHELX-97.[26] Interatomic distances and selected bond angles are listed in Table 1, and motifs of mutual adjunction[27] are displayed in Table 2. Details of the data collection and the structure refinement[28] are summarized in Table 3, atomic positions and coefficients of the isotropic thermal displacement parameters[29] are given in Table 4.

Further details on the crystal structure investigation may be obtained from the Fachinformationszentrum Karlsruhe, 76344 Eggenstein-Leopoldshafen, Germany (Fax: +49-7247-808-666; E-mail: crysdata@fiz-karlsruhe.de), on quoting the depository number CSD-419255 for La$_3$FMo$_4$O$_{16}$.

IR Spectroscopy: The infrared spectrum of La$_3$FMo$_4$O$_{16}$ was taken with a Nicolet 6700 FT-IR spectrometer equipped with an ATR unit using a diamond crystal, measuring the reflectance from the powdered samples.

Raman Spectroscopy: The bulk solid-state Raman spectrum of La$_3$FMo$_4$O$_{16}$ was recorded with a Nicolet Magna-IR 760 spectrometer with a FT-Raman Module attachment by use of a Nd:YAG excitation laser (wavelength: λ = 1064 nm).

UV/Vis Spectroscopy: The diffuse reflectance spectrum for La$_3$FMo$_4$O$_{16}$ has been recorded with a Varian Cary 500 Scan UV/Vis/NIR spectrophotometer equipped with a Praying Mantis accessory. A polytetrafluoroethylene standard was used as reference and the Kubelka–Munk function was applied to obtain band-gap information.[30] The band gap of La$_3$FMo$_4$O$_{16}$ was calculated to be 3.70 eV (335.5 nm). Hence, the absorption is situated in the UV range and the substance appears to be white.

Luminescence Spectroscopy: Photoluminescence spectra of La$_3$FMo$_4$O$_{16}$:Ce^{3+} and La$_3$FMo$_4$O$_{16}$:Pr^{3+} in the visible region were taken at room temperature with an Edinburgh Instruments FS900 spectrofluorimeter. This instrument is equipped with a xenon arc-

Table 3. Crystallographic data for the La$_3$FMo$_4$O$_{16}$.

	La$_3$FMo$_4$O$_{16}$
Crystal system, formula units	triclinic, $Z = 2$
Space group	$P\bar{1}$
Lattice parameters	
a/pm	724.86(2)
b/pm	742.26(2)
c/pm	1469.59(3)
α/deg	101.683(2)
β/deg	102.118(2)
γ/deg	100.276(2)
Calculated density, D_x/g cm^{-3}	4.849
Molar volume, V_m/cm^3 mol^{-1}	221.80
$F(000)$	952
Index range, $\pm h$ / $\pm k$ / $\pm l$	9 / 9 / 19
Theta range, $\theta_{\min}$.–$\theta_{\max}$./deg	2.88–28.28
Absorption coefficient, μ/mm^{-1}	11.88
Data corrections	background, polarization and Lorentz factors; numerical absorption correction with HABITUS[25]
Reflections, collected / unique	16834 / 3619
R_{int} / R_σ	0.084 / 0.049
Structure solution and refinement	program package SHELX-97,[26] scattering factors according to International Tables, vol. C[28]
R_1 for (#) reflections with $\|F_o\| \geq 4\sigma(F_o)$	0.024 (3157)
R_1 / wR_2 for all reflections	0.032 / 0.053
Goodness of Fit (GooF)	1.034
Extinction, g	0.0034(1)
Residual electron density, ρ/e$^-$ 10^{-6} pm^{-3}, min. / max.	1.00 / –1.41

Table 4. Atomic coordinates and equivalent isotropic thermal displacement parameters U_{eq}[a][29] for La$_3$FMo$_4$O$_{16}$ (all atoms at *Wyckoff* position 2i).

	x/a	y/b	z/c	U_{eq}/pm^2
La1	0.37266(4)	0.42349(4)	0.26080(2)	74(1)
La2	0.34196(4)	0.84605(4)	0.12265(2)	64(1)
La3	0.67308(4)	0.05017(4)	0.39467(2)	64(1)
F	0.4993(4)	0.2467(4)	0.7319(2)	120(6)
Mo1	0.23833(6)	0.27302(6)	0.01060(3)	64(1)
Mo2	0.16872(6)	0.90345(6)	0.33025(3)	73(1)
Mo3	0.77360(6)	0.24869(6)	0.17182(3)	72(1)
Mo4	0.20561(6)	0.42508(6)	0.51414(3)	64(1)
O1	0.4000(5)	0.2786(5)	0.9387(3)	158(9)
O2	0.0066(5)	0.1653(5)	0.9380(3)	170(8)
O3	0.2453(5)	0.5010(5)	0.0808(3)	153(8)
O4	0.3167(5)	0.1679(5)	0.1079(3)	114(7)
O5	0.1152(6)	0.6946(6)	0.2408(3)	209(9)
O6	0.0346(5)	0.0303(6)	0.6395(3)	180(8)
O7	0.3413(5)	0.8866(5)	0.4321(3)	134(8)
O8	0.3124(5)	0.0694(5)	0.2851(3)	121(7)
O9	0.6817(5)	0.4481(5)	0.2008(3)	164(8)
O10	0.0258(5)	0.2950(5)	0.2150(3)	189(9)
O11	0.7106(6)	0.1548(6)	0.0473(3)	210(9)
O12	0.6573(5)	0.0756(5)	0.2240(3)	117(7)
O13	0.3018(5)	0.2401(5)	0.5432(3)	194(9)
O14	0.2625(5)	0.4474(6)	0.4074(3)	179(8)
O15	0.9492(5)	0.3265(5)	0.4982(3)	137(8)
O16	0.6440(5)	0.3798(5)	0.3866(3)	137(8)

[a] U_{eq} is defined as the 1/3 of the trace of the orthogonalized U_{ij} tensor.

lamp, a microsecond flashlamp (pulse length: 2 µs) and a red-sensitive photomultiplier (300–850 nm).

EPR Spectroscopy: EPR spectra in the X band were recorded with a Bruker System EMX connected to a Oxford ITC 4 temperature controller.

Supporting Information (see also the footnote on the first page of this article): Diffuse reflectance spectrum, experimental and theoretical powder diffractogram of $La_3FMo_4O_{16}$.

Acknowledgments

[1] Th. Schleid, S. Strobel, P. K. Dorhout, P. Nockemann, K. Binnemans, I. Hartenbach, *Inorg. Chem.* **2008**, *47*, 3728–3735.
[2] E. Cavalli, P. Boutinaud, T. Cucchietti, M. Bettinelli, *Opt. Mater.* **2009**, *31*, 470–473.
[3] Yu. K. Voron'ko, E. V. Zharikov, D. A. Lis, A. V. Popov, V. A. Smirnov, K. A. Subbotin, M. N. Khromov, V. V. Voronov, *Opt. Spectrosc.* **2008**, *105*, 538–546.
[4] R. G. Dickinson, *J. Am. Chem. Soc.* **1920**, *42*, 85–93.
[5] I. Hartenbach, S. Strobel, P. K. Dorhout, Th. Schleid, *J. Solid State Chem.* **2008**, *181*, 2828–2836.
[6] I. Hartenbach, S. Strobel, Th. Schleid, K. Krämer, P. K. Dorhout, *Z. Anorg. Allg. Chem.* **2009**, *635*, 966–975.
[7] I. Hartenbach, Th. Schleid, *Z. Anorg. Allg. Chem.* **2009**, *635*, 1904–1909.
[8] I. Hartenbach, S. Strobel, Th. Schleid, P. K. Dorhout, *Z. Anorg. Allg. Chem.*, DOI: 10.1002/zaac.200900572.
[9] I. Hartenbach, unpublished results, University of Stuttgart.
[10] W. Jeitschko, *Acta Crystallogr., Sect. B* **1973**, *29*, 2074–2081.
[11] A. Zalkin, D. H. Templeton, T. E. Hopkins, *Inorg. Chem.* **1966**, *5*, 1466–1468.
[12] W. C. Köhler, E. O. Wollan, *Acta Crystallogr.* **1953**, *6*, 741–742.
[13] R. Hoppe, *Z. Kristallogr.* **1979**, *150*, 23–52.
[14] I. Hartenbach, *Z. Anorg. Allg. Chem.* **2008**, *634*, 2044–2044.
[15] D. B. Brown, J. A. Zubieta, P. A. Vella, J. T. Wrobleski, T. Watt, W. E. Hatfield, P. Day, *Inorg. Chem.* **1980**, *19*, 1945–1950.
[16] I. D. Brown, D. Altermatt, *Acta Crystallogr., Sect. B* **1985**, *41*, 244–247.
[17] N. E. Brese, M. O'Keeffe, *Acta Crystallogr., Sect. B* **1991**, *47*, 192–197.
[18] M. S. Wickleder, I. Göhausen, *Z. Anorg. Allg. Chem.* **2000**, *626*, 1725–1727.
[19] I. Krügermann, M. S. Wickleder, *J. Solid State Chem.* **2002**, *167*, 113–118.
[20] C. Lipp, Th. Schleid, *Z. Anorg. Allg. Chem.* **2008**, *634*, 1662–1668.
[21] C. Lipp, Ph.D. Thesis, University of Stuttgart, **2008**.
[22] I. P. Swainson, M. T. Dove, D. C. Palmer, *Phys. Chem. Miner.* **2003**, *30*, 353–365.
[23] G. Busca, *J. Raman Spectrosc.* **2002**, *33*, 348–358.
[24] M. Maczka, K. Hermanowicz, J. Hanuza, *J. Mol. Struct.* **2005**, *744–747*, 283–283.
[25] W. Herrendorf, H. Bärnighausen, *HABITUS*, program for the optimization of the crystal shape for numerical absorption correction in X-SHAPE (version 1.06, Stoe, Darmstadt, **1999**), Karlsruhe, Gießen, **1993**, **1996**.
[26] G. M. Sheldrick, *SHELX-97*, program package for solution and refinement of crystal structures from X-ray diffraction data, Göttingen, **1997**.
[27] R. Hoppe, *Adv. Fluorine Chem.* **1970**, *6*, 387–438; *Izv. Jugoslav. Centr. Krist. (Zagreb)* **1973**, *8*, 21–36; *Crystal Structure and Chemical Bonding in Inorganic Chemistry* (Eds.: C. J. M. Rooymans, A. Rabenau), Amsterdam, **1975**, pp. 127.
[28] Th. Hahn, A. J. C. Wilson, *International Tables for Crystallography*, vol. C, 2nd ed., Kluwer Academic Publishers, Boston, Dordrecht, London, **1992**.
[29] R. X. Fischer, E. Tillmanns, *Acta Crystallogr., Sect. C* **1988**, *44*, 775–776.
[30] W. W. Wendlandt, H. G. Hecht, *Reflectance Spectroscopy*, Interscience Publishers, New York, **1966**.